

## Reservoir Characterization Of The ‘Pira\_J’ Field, Deepwater Offshore Niger Delta, Nigeria: A Seismic Attribute And Petrophysical Approaches.

Jaff, Victor Sewong<sup>1</sup>; Nfor, Bruno Ndicho<sup>2</sup>; and Ikomi, Kelvin Misan<sup>3</sup>

<sup>1</sup>Department of Geology, Chukwuemeka Odumegwu Ojukwu University, Uli, Anambra State, Nigeria.

<sup>2</sup>Department of Geology, Chukwuemeka Odumegwu Ojukwu University, Uli, Anambra State, Nigeria

<sup>3</sup>Department of Geology, Chukwuemeka Odumegwu Ojukwu University, Uli, Anambra State, Nigeria

---

### Abstract

This research work focused on characterizing the reservoir rocks, defining the stratigraphic and structural pattern of the Pira\_J field deep water offshore Niger Delta Basin, Nigeria using seismic and well data from five wells. In order to achieve this, seismic attributes and petrophysical analyses were integrated using the PETREL Software. Seven hydrocarbon reservoir bearing units, namely RES\_01, RES\_02, RES\_03, RES\_04, RES\_05, RES\_06 and RES\_07 were identified from wireline logs. Out of the seven reservoir tops-tie-to-seismic horizons, only five were mapped out (because they contained all the needed data) to create time structural maps. The time structural maps were then converted to depth structural maps with the aid of a polynomial function from checkshot data. Results show that, the computed petrophysical properties for the reservoir units have average hydrocarbon saturation ranging from 0.5 to 0.9, effective porosity ranging from 0.14 to 0.34, permeability ranging from 23 mD to 793 mD and net to gross ranging from 0.6 to 0.95. Fifteen faults; listric, antithetic, synthetic and collapse crest faults were identified, mostly dipping in the NE to SW together with a rollover anticlinal structure. Channels, however, were also identified trending in the NE-SW creating reservoirs fairway. Extracted RMS and minimum interval attributes for both near-angle and far-angle stack seismic show the distribution and architecture of the sand fairway with far-angle stack attributes showing the fluid effect, basically oil. This depicts characteristics of class 3 AVO (Amplitude Versus Offset) attributes. Consequently, the field shows good reservoir qualities saturated with hydrocarbon from both petrophysical and attribute analyses. Nevertheless, marine shales intercalating some of reservoir units may baffle fluid flow vertically and create fluid flow variations in the reservoir units.

**Keywords:** Petrophysical analysis, Seismic attribute, Reservoir characterization, Deep-water, AVO.

---

Date of Submission: 08-06-2023

Date of Acceptance: 18-06-2023

---

### I. INTRODUCTION

The global demand for energy will keep on increasing with a continual growth in population especially in developing countries like Nigeria. The United Nation (2017) forecasts that the world's population will be 9.8 billion in the year 2050 and with Africa and Asia having the biggest population growth. However, the British Petroleum (2018), ExxonMobil (2018) and International Energy Agency (2018) suggest that the quest for energy may not essentially be due to population growth but improvement in living standard of developing countries (Africa and Asia specifically). Thereby influencing the future energy demand. Sources and production of energy are predicted to vary as we move towards net-zero by 2050. Despite the projection of net-zero scenarios, oil and gas will still account for 55% of the energy mix in 2050 (ExxonMobil, 2022). According to the ExxonMobil (2022), the energy outlook will increase by 15% in the year 2050 compare with today's population. Therefore, the continual increase in energy demand is weighing down on petroleum industries to catch up with the energy demand. Thus, it is imperative to increase upstream activities in frontier provinces like the deep water. The petroleum elements in deep waters, however, are difficult to evaluate due to the complex geological condition. Consequently, it is important to employ the right technology to drill and target the hydrocarbon prospect regardless of financial risk associated with it (Joye 2015; Skogdalen and Vinnem 2012; Bell *et al.*, 2005; Reader and O'Connor, 2014).

The aim of this study is to characterize the reservoir rocks, define the stratigraphic and structural pattern of the ‘Pira-J’ field deep offshore Niger Delta Basin, Nigeria. This will be achieved by defining, identifying and outlining the reservoir rock units, computing intrinsic reservoir properties, identifying faults and extracting attributes in order to characterize the reservoir units and define the structural and stratigraphic pattern of the study area. Nonetheless, deep water exploratory activities are very expensive and have high degree of

uncertainty in determining the presence, distribution and quality of reservoir to enhance hydrocarbon recovery. In this regard Petrel software considered a right technology, and the cost-effective method was used.

Principally, seismic attributes define the structural and stratigraphic pattern of the subsurface, and the physical characters of rock-fluid, since they have good relationship with pore fluids properties, lithology and ends of hydrocarbon water boundary (Chopra and Marfurt 2005; Bodine 1984, 1986; Taner, 2001). According to Taner *et al* (1994), seismic attributes are classed into physical and geometrical attributes. Physical attributes are associated with pore fluids, changes in depositional environment and lithology. Geometric attributes improve the azimuth, continuity and dip characteristics. Physical parameters such as velocity, reflection geometry, and acoustic impedance affect absorption and thus give structural information or act as Direct Hydrocarbon Indicators. These attributes are thus used to characterized and predict reservoir properties of the targeted zone.

#### Field location and geologic setting of the study area

The Cenozoic Niger Delta Basin is one of leading regressive basin in the world and occupies a land mass of about 75000 km<sup>2</sup> within latitude 40 and 60'N and longitude 30 and 90' E (Doust and Omatsola, 1990). The basin is found within the Gulf of Guinea on the West Africa margin (Doust and Omatsola, 1990). Our study area falls within the deep-water of the Niger Delta Basin (Figure 1).

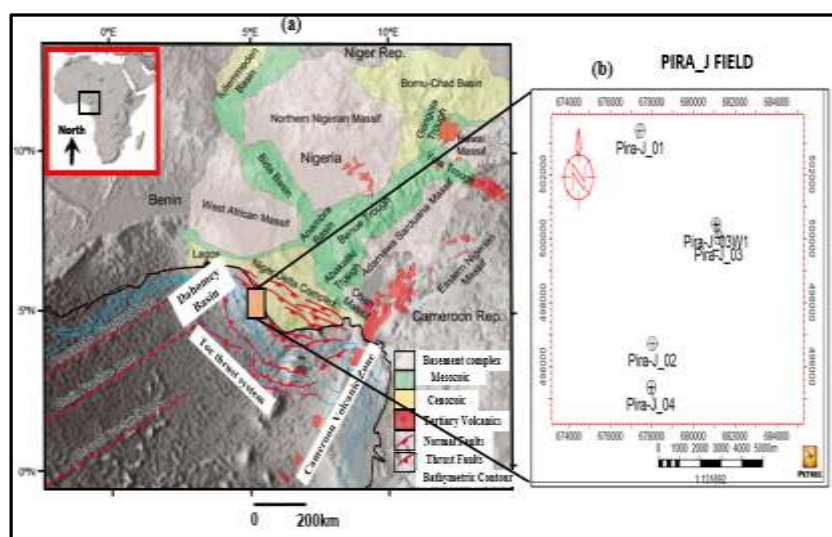


Figure 1: Location of the Study Area (modified from Onuoha, 1999).

The Niger Delta is located in the Gulf of Guinea on the margin of West Africa (Figure 1). It is one of the biggest regressive deltas in the world (Doust and Omatusola, 1990) and is considered as a classical shale tectonic province (Wu and Bally, 2000). The basin is bordered by the Cameroon Volcanic Line, CVL to the East, the Dahomey Basin to the West and 13100 ft Bathymetric contour (Figure 1). The shape and structure of the Niger delta basin is controlled by the fracture zones along the oceanic crust such as the charcot fracture zone (Figure 1) exhibited as trenches and ridges that formed during the opening of the South Atlantic in the Early Jurassic to Cretaceous. The Delta sits on the South end of the Benue Trough, the failed armed of the rift tippie junction. After rifting stopped in the Late Cretaceous (Lehner and De Ruitter, 1977), marginal failure caused by gravity tectonics became the dominant deformation mechanism in the basin. Internal deformation mechanisms caused by shale mobility occurred due to two processes (Kulke, 1995). First, the instability of the slope developed due to absent of basinward, lateral and support for the delta slope clay (AakataFm) which are under compacted. Secondly, the formation of shale diapers from the loading of the over pressured, poorly compacted, delta-slope clays and prodelta of the Akata Formation by the higher density delta-front sands of the Abdada Formation.

Traps in the Niger Delta Basin are mainly, structural, stratigraphic and combination traps. According to Stacher (1995), Evamy *et al.* (1978) structural traps were formed during syndimentary deformation of the Agbada sequence. These structural traps are mainly antithetic faults, collapse crest fault, growth faults and rollover structures (Doust and Omatsola, 1990).

The sequence stratigraphy of the Niger Delta is partitioned into three key formations (Figure 2); Akata, Agbada and Benin Formations. These formations demonstrate a depositional facies that are prograding, differentiated on the basis of sand to shale ratios. According to Short and Stäuble, 1967 and summarized in a variety of papers (e.g. Kulke, 1995; Doust and Omatola, 1990; Avbobvo, 1978). The Akata Formation is characterized by thick shale sequence (potential source rock), minor amount of clay and silt and may have turbidite sand (potential reservoir rock) and is found at the base of the basin. According to Doust and Omatsola (1990), the formation has a thickness of about 7000 m. Probably, deep sea fan sands that may be present in the Akata Formation were deposited by turbidity current during the formation of the delta (Burke, 1972). The Agbada Formation is of Eocene to Recent and is characterized by parallel siliciclastic sediments with a thickness of over 3700 m. The environments of deposition is made up of fluvio-deltaic, delta front and delta-topset. The formation is regarded as a key hydrocarbon bearing unit with alternation of sandstone and shale constituting the reservoir and source rocks of the Niger Delta Basin. The Benin Formation overlies the Agbada Formation with environment of deposition mainly continental; coastal plain and alluvial and a thickness of up to 2000 m (Avbobvo, 1978).

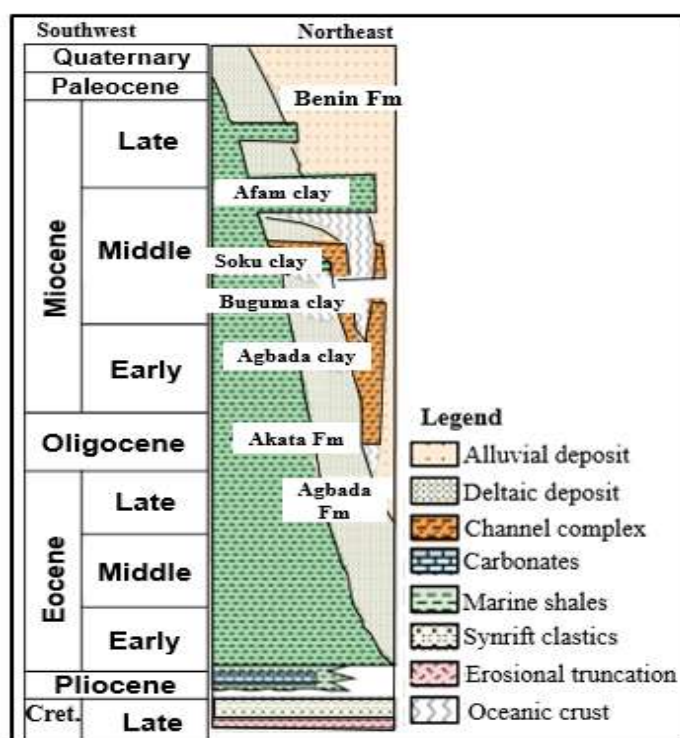


Figure 2: General Lithostratigraphy of the Niger Delta Basin (modified from Lawrence *et al.*, 2002).

## II. MATERIALS AND METHODS

For this study, well information and 3-D seismic cube in SEG-Y format (Table 1) were integrated in other to characterize the reservoirs of interest, define the stratigraphic and structural pattern of study area. The software used for this study is Petrel 2018 E and P together with Microsoft excel 2013.

Both well data and seismic data were quality checked first, followed by reservoir tops identification and correlation of the reservoirs across the wells. Petrophysical properties of the identified reservoirs were computed. Synthetic seismogram was then generated to tie the well data given in depth to seismic data given in time. Structural and stratigraphic interpretation of faults and horizons were then carried out with the time maps generated and converted to depth maps using a second order polynomial function. Seismic attributes were extracted from the time structural maps in order to define the stratigraphic and structural pattern of the study area.

**Table 1: Data used for the study**

Information	Pira_J 1	Pira_J 2	Pira_J 3	Pira_J 3W	Pira_J 4
Gamma ray log	√	√	√	√	√
Resistivity log	√	√	√	√	√
Neutron log	√	√	√	√	√
Density log	√	√	√	√	√
Sonic log	√	√	√	√	√
Checkshot	√	√	√	√	√
Deviation	√	√	√	√	√
Well head	√	√	√	√	√
3-D seismic cube	√	√	√	√	√

For qualitative analysis, the gamma ray log was used to discriminate sand and shale, setting a shale baseline of 70 API where negative deflection indicates sand and positive deflection indicates shale. Low gamma ray and high resistivity values in both gamma ray log and resistivity logs respectively indicates hydrocarbon bearing units couple with neutron-density log cross plot. For quantitative analysis, petrophysical parameters such as water saturation, permeability, volume of shale, gamma ray index, porosity and net-to-gross (NTG) together with volume of hydrocarbon in place were calculated.

**Volume of shale**

The shale volume delimited within the reservoir unit was determined to enable the estimation of other parameter like effective porosity using equation 2 for Tertiary and unconsolidated sediments by Dresser Atlas (1979). But firstly, the gamma ray index is computed using equation 1 below.

$$I_{GR} = \frac{GR_{log} - GR_{min}}{GR_{max} - GR_{min}} \dots\dots\dots (1)$$

$I_{GR}$  = gamma ray index,  $GR_{log}$  = readings from the gamma ray log,  $GR_{max}$  = maximum gamma ray reading, and  $GR_{min}$  = minimum gamma ray reading.

$$V_{sh} = 0.083 * (2^{3.7+I_{GR}} - 1) \dots\dots\dots (2)$$

**Porosity**

Porosity was obtained from any of the porosity logs; density, neutron and sonic logs. These logs are sensitive to the nature of the saturated fluids within the pore investigated by the tool. Combination of two porosity logs can detect the presence of gas or light oil in the formation. The density log was used to derived porosity using equation 3 below

$$\emptyset = \frac{\rho_{matrix} - \rho_{log}}{\rho_{matrix} - \rho_{fluid}} \dots\dots\dots (3)$$

Where porosity obtained from density log,  $\rho_{matrix}$  =rock matrix density,  $\rho_{fluid}$  = fluid density,  $\rho_{log}$  = readings from density log

**Effective porosity**

Effective porosity is the outcome of the removal of the shale/clay effect in the reservoir unit as shown in equation 2. It is made up of pore spaces that are connected to each other, easing the flow of fluid within the reservoir unit, unlike total porosity that contains even fluid in the voids that cannot flow or escaped.

$$\emptyset_e = 1 - V_{sh} * \emptyset_t \dots\dots\dots (4)$$

$\emptyset_e$  = effective porosity,  $V_{sh}$  = volume of shale, and  $\emptyset_t$  = total porosity

**Formation resistivity factor**

The Humble equation was used to calculate the formation factor. It is simply the ratio of resistivity of formation to resistivity of formation water and is constant despite the fluid occupying the pores. It is affected or influent mainly by texture together with composition, size, arrangement and orientation of the matrix.

$$F = \frac{a}{\emptyset^m} \dots\dots\dots (5)$$

Where a = tortuosity factor

m= cementation factor

$\emptyset$ = porosity where a =0.62. m = 2.15

**Water saturation**

The saturation of each formation was estimated with the aid of Archie's (1942) equation which shows the portion of the rock filled by water. This equation is an estimation of hydrocarbon saturation in the pore spaces of rock and consequently volume of hydrocarbon initially in place.

$$S_w = (F * \frac{R_w}{R_t})^{1/n} \dots\dots\dots (6)$$

Where F= Formation factor, R<sub>w</sub>= Formation water resistivity at formation temperature, R<sub>t</sub>= True formation resistivity and n= saturation exponent.

**Permeability**

Permeability of a formation is influenced by pore size, and shape as well as the continuity of these properties together with porosity. Shale/clay are porous but exhibit zero permeability due of lack of interconnect pore spaces causing fluid not to flow through them. Absolute permeability is computed using equation 7 or 8 with the aid of irreducible water formation predicted from equation 9.

$$k^{1/2} = \frac{100 * \emptyset^{2.25}}{S_{wirr}} \dots\dots\dots (7)$$

$$K^{1/2} = \frac{250 * \emptyset^3}{S_{wirr}} \dots\dots\dots (8)$$

$$S_{wirr} = (\frac{F}{2000})^{1/2} \dots\dots\dots (9)$$

Portion of the effective porosity that contains water that will not flow out of the rock

$$K_{rw} = (\frac{S_w - S_{wirr}}{1 - S_{wirr}})^3 \dots\dots\dots (10)$$

$$K_{ro} = \frac{(1 - S_{wirr})^{2.1}}{(1 - S_{wirr})^2} \dots\dots\dots (11)$$

K= permeability, S<sub>wirr</sub>= irreducible water formation, Ø = porosity, S<sub>w</sub> = water saturation, F= formation resistivity factor.

**III. DISCUSIONS AND RESULTS**

**Lithostratigraphic correlation**

From the well log correlation study, seven hydrocarbon bearing reservoir units (RES\_01, RE\_02, RES\_03, RES\_04, RES\_05, RES\_06 and RES\_07) were identified across 'Pira\_J' field to know the vertical and horizontal extend of these reservoirs (Figure 3). However, two reservoirs, RES\_03 and RES\_07 are not continuous and present only in well Pira\_J 01. Reservoir RES\_01, and RES\_02 are only penetrated by wells Pira\_J\_01 and Pira\_J 02, RES\_05 and RES\_06 truncate in the N direction and is absent in well Pira\_J 01 (Figure 3). Only reservoir RES\_04 is laterally extensive across the field and is present in all wells except for well Pira\_J 03 that is shallower and didn't penetrate that interval (Figure 3). Within the units of interest, low gamma ray values, high resistivity values and cross plot of neutron-density logs are depicted by the gamma ray, resistivity and combination of neutron-density logs respectively (Figure 3). However, oil water contact (OWC) are also identified by low resistivity values and sidetrack of the neutron-density logs within the reservoir.

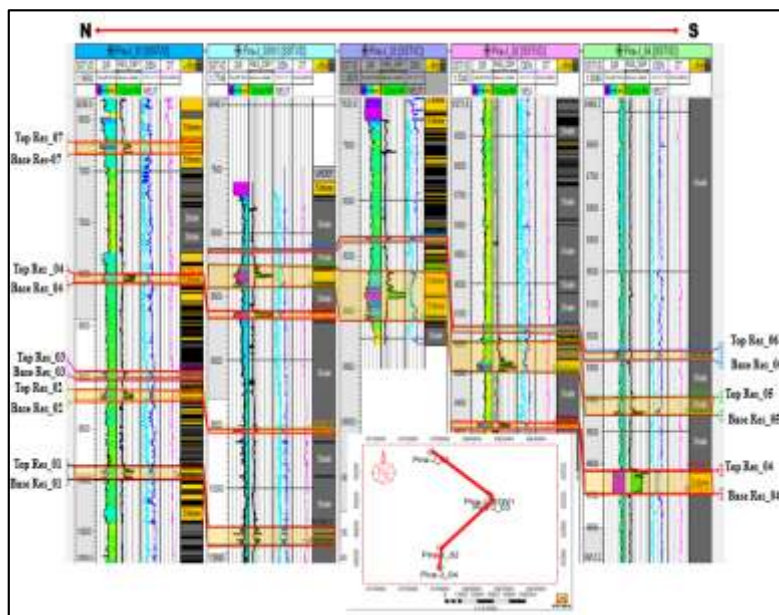


Figure 3: Reservoir correlation of the wells in Pira\_J Field

#### Petrophysical analysis

For petrophysical analysis, all calculations were carried out using the relevant equations discussed previously and presented in tables 2, 3, 4, 5, 6, 7, and 8.

Reservoir RES\_01 petrophysical results are presented in table 2 below. The reservoir unit is penetrated by only two wells, Pira\_J 01 and Pira\_03W within a depth interval of 10302.86 ft to 10445.1 ft and 9860.11 ft to 9989.59 ft respectively. The thickness of the reservoir ranges from 142.26 ft in Pira\_J-01 to 129.48 ft in Pira\_J-03W with a mean thickness of 135.87 ft. It has an average permeability of 63.85 mD, average total porosity of 0.20, and effective porosity of 0.15, volume of shale 0.32, net to gross of 0.68, water saturation of 0.46 and hydrocarbon saturation of 0.54. The formation factor ranges from 148.16 in Pira\_J 01 to 34.11 in Pira\_J 03W. The formation factor is high in Pira\_J-01 due to the present of marine shale which may baffle fluid flow.

Reservoir RES\_02 petrophysical results are displayed in Table 3. The reservoir unit is also penetrated by only wells Pira\_J 01 and Pira\_J 03W with a reservoir thickness of 97.94 ft and 34.01 ft respectively within a depth range of 9529.91 ft to 9563.92 ft in Pira\_J 03W and 9121.21 ft to 9219.15 ft in Pira\_J 01. The reservoir is characterized by an average hydrocarbon saturation ranging from 0.57 to 0.64, average permeability ranging from 262.04 mD to 150.49 mD, average effective porosity of 0.20 to 0.22, average shale volume of 0.15 to 0.18 and an average net to gross of 0.82 to 0.85.

Reservoir RES\_03 petrophysical results are displayed in Table 4. The reservoir unit is not laterally extensive and is present only in well Pira\_J 01 at a depth interval of 8945.58 ft to 9016.52 ft with a thickness of 70.94 ft. It has an average formation factor of 25.24, average permeability of 151.98 mD of average total porosity of 0.25, average effective porosity of 0.20, average water saturation of 0.54, average hydrocarbon saturation of 0.46, and average volume of shale of 0.21.

The petrophysical results of reservoir RES\_04 are presented in Table 5. The reservoir unit is laterally extensive across the wells except for well Pira\_J 03 that didn't penetrate the reservoir depth. This reservoir has the best petrophysical properties compare to other reservoir units and it was penetrated at a depth interval of 8000.13 ft to 8079.19 ft in Pira\_J 01, 9469.02 ft to 9486.02 ft in Pira\_J 02, 8609.58 ft to 8663.44 ft in Pira\_J 03W and 9620.1 ft to 9693 ft in Pira\_J 04 with a thickness of 79.06 ft, 18 ft, 53.86 ft and 72.9 ft respectively. The reservoir unit is characterized by an average effective porosity ranging from 0.30 to 0.26, average permeability ranging from 776.87 mD to 429.33mD, average formation factor of 8.68 to 13.54, average hydrocarbon saturation of 0.92 to 0.83, average net to gross of 0.83 to 0.89 and average volume of shale ranging from 0.11 to 0.17.

Reservoir RES\_05 petrophysical results are presented in Table 6. The reservoir unit is penetrated at a depth interval of 9145.66 ft to 9161.79 ft, 8130.55 ft to 8144.19 ft, 8128.37 ft to 8140.37 ft and 9246.4 ft to 9273.7 ft in wells Pira\_J 02, 03, 03W and 04 respectively. The reservoir unit truncates in the N direction (Figure 3) and is absent in well Pira\_J 01. It has a thickness of 104.37 ft, 178.26 ft, 170.68 ft, and 57.94 ft in wells Pira\_J 02, 03,

03W and 04 respectively. The average effective porosity varies between 0.15 and 0.24, average permeability ranges from 94.07 mD to 368.28 mD and average hydrocarbon saturation ranging from 0.61 to 0.74.

In reservoir RES\_06, the reservoir is laterally extensive except in well Pira\_J 01 due to the fact that it truncates in the northern direction. The reservoir petrophysical results are presented in table 07 below with average effective porosity ranging from 0.15 to 0.28 and average permeability ranging from 42.21 mD to 915.38 mD. The reservoir has a thickness of 16.13 ft, 13.64 ft, 12 ft and 27.3 ft in wells Pira\_J 02, 03, 03W and 04 respectively. Well Pira\_J 02 is completely wet and is water saturated. The reservoir has a net to gross ranging from 0.71 to 0.85, volume of shale ranging from 0.15 to 0.29 and hydrocarbon saturation varying between 0.53 and 0.23.

Reservoir RES\_07 is only identified in well Pira\_J 01 within a depth range of 6730.86 ft to 6828.4 ft and having a thickness of 97.57. The reservoir has an average water saturation of 0.36, average hydrocarbon saturation of 0.64, average total porosity of 0.30, average effective porosity of 0.27, average shale volume of 0.10, average net to gross of 0.90, average permeability of 387.78 mD and average formation factor of 10.53. The results are presented in table 8 below.

Permeability versus effective porosity (Figure 4) for reservoir RES\_04 was plotted and the result showed a linear relationship with the maximum value of porosity 40% (0.40) and permeability 2129.07 mD.

**Table 2: Average petrophysical properties for reservoir RES\_01**

RES_01											
WELLS	TVDS/ Ft		Thickness Ft	Vsh Frac	NTG Frac	phit Frac	phie Frac	Perm mD	F /	S <sub>w</sub> Frac	S <sub>h</sub> Frac
	TOP	BASE									
Pira_J-04	/	/	/	/	/	/	/	/	/	/	/
Pira_J 03W	-10302.86	-10445.1	142.26	0.44	0.56	0.18	0.12	41.26	148.16	0.45	0.55
Pira_J 03	/	/	/	/	/	/	/	/	/	/	/
Pira_J 02	/	/	/	/	/	/	/	/	/	/	/
Pira_J01	-9860.11	-9989.59	129.48	0.19	0.81	0.21	0.18	86.43	34.11	0.47	0.53
Averages			135.87	0.32	0.68	0.20	0.15	63.85	91.13	0.46	0.54

**Table 3: Average petrophysical properties for reservoir RES\_02**

RES_02											
WELLS	TVDS/ Ft		Thickness Ft	Vsh Frac	NTG Frac	phit Frac	phie Frac	Perm mD	F /	S <sub>w</sub> Frac	S <sub>h</sub> Frac
	TOP	BASE									
Pira_J 04	/	/	/	/	/	/	/	/	/	/	/
Pira_J 03W	-9529.91	-9563.92	34.01	0.18	0.82	0.25	0.22	262.04	11.19	0.43	0.57
Pira_J 03	/	/	/	/	/	/	/	/	/	/	/
Pira_J 02	/	/	/	/	/	/	/	/	/	/	/
Pira_J01	-9121.21	-9219.15	97.94	0.15	0.85	0.24	0.20	150.49	21.45	0.36	0.64
Average			65.97	0.17	0.83	0.25	0.21	206.26	16.32	0.40	0.60

**Table 4: Average petrophysical properties for reservoir RES\_03**

RES_03											
WELLS	TVDS/ Ft		Thickness Ft	Vsh Frac	NTG Frac	phit Frac	phie Frac	Perm mD	F /	S <sub>w</sub> Frac	S <sub>h</sub> Frac
	TOP	BASE									
Pira_J 04	/	/	/	/	/	/	/	/	/	/	/
Pira_J 03W	/	/	/	/	/	/	/	/	/	/	/
Pira_J 03	/	/	/	/	/	/	/	/	/	/	/
Pira_J 02	/	/	/	/	/	/	/	/	/	/	/
Pira_J01	-8945.58	-9016.52	70.94	0.21	0.79	0.25	0.20	151.98	25.24	0.54	0.46
Average			70.94	0.21	0.79	0.25	0.20	151.98	25.24	0.54	0.46

**Table 5: Average petrophysical properties for reservoir RES\_04**

RES_04											
WELLS	TVDS/ Ft		Thickn ess Ft	Vsh Frac	NTG Frac	phit Frac	phie Frac	Perm mD	F /	S <sub>w</sub> Frac	S <sub>h</sub> Frac
	TOP	BASE									
Pira_J 04	-9620.1	-9693	72.9	0.17	0.83	0.35	0.29	561.04	8.87	0.08	0.92

Reservoir Characterization Of The 'Pira\_J' Field, Deepwater Offshore Niger Delta, Nigeria....

Pira_J 03W	-8609.58	-8663.44	53.86	0.16	0.84	0.34	0.29	776.87	10.08	0.15	0.85
Pira_J 03	/	/	/	/	/	/	/	/	/	/	/
Pira_J 02	-9468.02	-9486.02	18	0.11	0.89	0.30	0.26	429.33	13.54	0.17	0.83
Pira_J01	-8000.13	-8079.19	79.06	0.11	0.89	0.34	0.30	637.60	8.68	0.12	0.88
Average			55.95	0.14	0.86	0.33	0.29	601.21	10.29	0.13	0.87

Table 6: Average petrophysical properties for reservoir RES\_05

RES_05											
WELLS	TVDS/ Ft		Thickness	Vsh	NTG	phit	phie	Perm	F	S <sub>w</sub>	S <sub>h</sub>
	TOP	BASE	Ft	Frac	Frac	Frac	Frac	mD	/	Frac	Frac
Pira_J 04	-9390.7	-9448.64	57.94	0.42	0.53	0.25	0.15	94.07	63.27	0.39	0.61
Pira_J 03W	-8255.23	-8425.91	170.68	0.18	0.82	0.27	0.22	165.14	18.17	0.26	0.74
Pira_J 03	-8255.17	-8433.43	178.26	0.12	0.88	0.34	0.29	787.98	11.19	0.29	0.71
Pira_J 02	-9192.6	-9296.97	104.37	0.22	0.78	0.30	0.24	368.28	19.33	0.36	0.64
Pira_J01	/	/	/	/	/	/	/	/	/	/	/
Average			127.81	0.24	0.76	0.28	0.22	353.87	27.99	0.33	0.67

Table 7: Average petrophysical properties for reservoir RES\_06

RES_06											
WELLS	TVDS/ Ft		Thickness	Vsh	NTG	phit	Phie	Perm	F	S <sub>w</sub>	S <sub>h</sub>
	TOP	BASE	Ft	Frac	Frac	Frac	Frac	mD	/	Frac	Frac
Pira_J 04	-9246.4	-9273.7	27.3	0.29	0.71	0.27	0.19	138.87	33.08	0.77	0.23
Pira_J 03W	-8128.37	-8140.37	12	0.24	0.76	0.34	0.27	680.05	19.23	0.48	0.52
Pira_J 03	-8130.55	-8144.19	13.64	0.15	0.85	0.33	0.28	915.38	15.18	0.47	0.53
Pira_J 02	-9145.66	-9161.79	16.13	0.25	0.75	0.20	0.15	42.2	41.21	/	/
Pira_J01	/	/	/	/	/	/	/	/	/	/	/
Average			17.2	0.23	0.76	0.29	0.22	444.13	27.17	0.58	0.42

Table 8: Average petrophysical properties for reservoir RES\_07

WELLS	TVDS/ Ft		Thickness	Vsh	NTG	phit	phie	Perm	F	S <sub>w</sub>	S <sub>h</sub>
	TOP	BASE	F	Frac	Frac	Frac	Frac	mD	/	Frac	Frac
Pira_J 04	/	/	/	/	/	/	/	/	/	/	/
Pira_J 03W	/	/	/	/	/	/	/	/	/	/	/
Pira_J 03	/	/	/	/	/	/	/	/	/	/	/
Pira_J 02	/	/	/	/	/	/	/	/	/	/	/
Pira_J01	-6730.83	-6828.4	97.57	0.10	0.89	0.30	0.27	387.78	10.53	0.36	0.63
Average			97.57	0.10	0.90	0.30	0.27	387.78	10.53	0.36	0.64

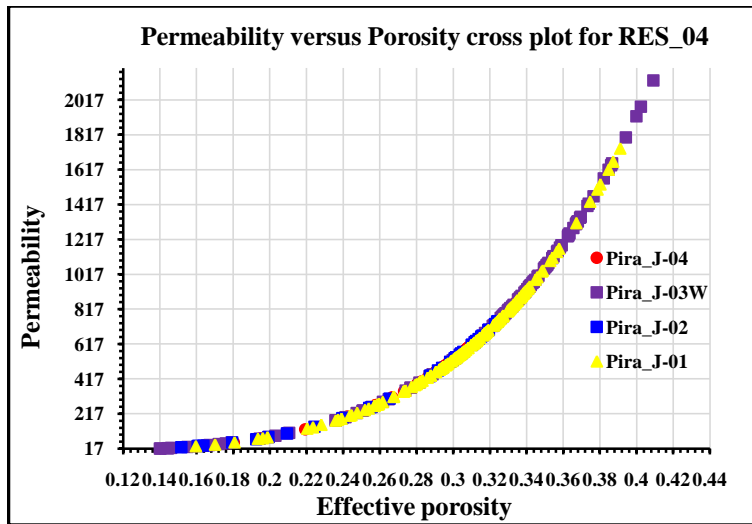


Figure 4: Permeability versus effective porosity cross plot for reservoir RES\_04 interval.

#### Seismic-to-well tie

A synthetic seismogram was generated using well Pira\_J-01 (Figure 6) through the method of creating a relationship between well information given in depth and seismic data given in time (well to seismic tie). This was done by first calibrating sonic (1/velocity) log and check shot in order to avoid spurious and pitfalls information. Thereafter, checkshot was used together with sonic and density logs to generate synthetic seismogram through the process where product of the density and sonic logs gave the acoustic impedance. The acoustic impedance was then used to generate the reflection coefficient that was convolved with zero phase ricker 25 Hz frequency (extracted from the seismic data) in order to generate a synthetic seismogram. Based on the well to seismic tie, a bulk shift of 10 ms was performed to tie the geologic response of the seismic data and synthetic seismogram (gotten from well data). From the relationship between well data and seismic data carried out, the tops of the reservoir of interest matches with the trough on the seismic section. The synthetic seismograms for the rest of the wells were generated and tie to the seismic data and the result were similar to well Pira\_J-01 and seismic data using same parameters.

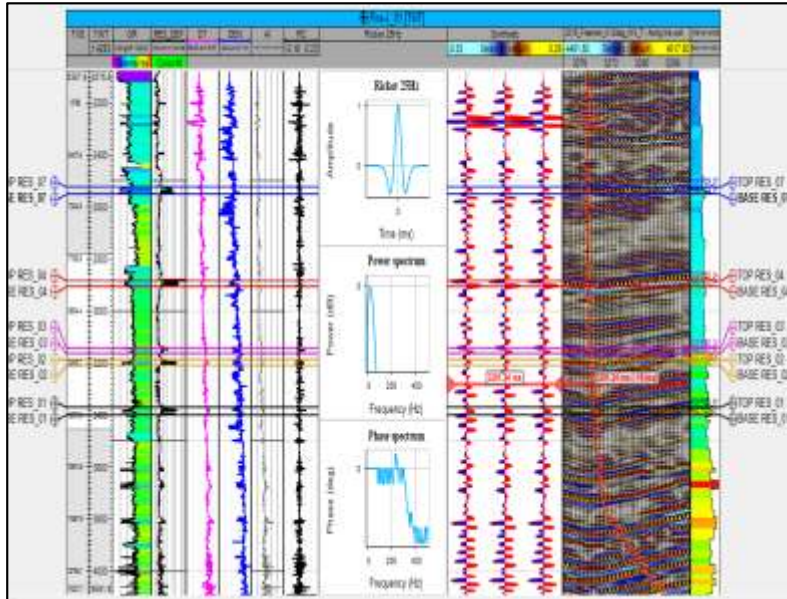


Figure 5: Seismic to well tie using well Pira-J\_01

**Seismic structural and stratigraphic interpretation**

Reflection events connected with the key geologic reservoirs were identified using well log data and delineated across the field (seismic data). The interpretation of the seismic was focused on reflectors from sea bed to the top of reservoir Res\_01 at -3407.76 ms TWT (Figure 7a and 7b).

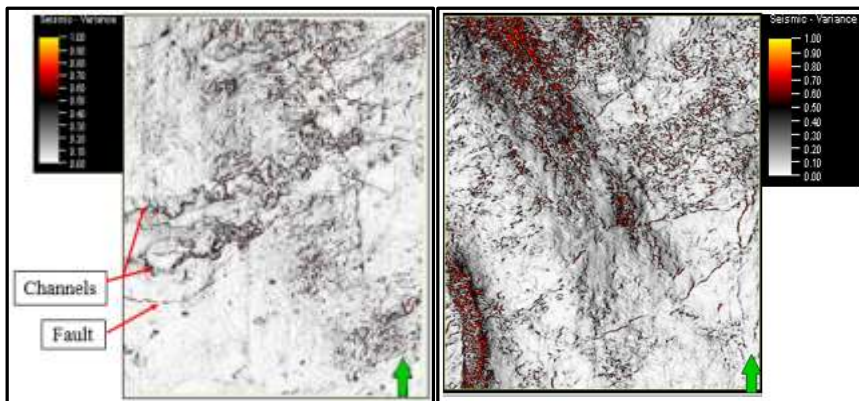


Figure 6 (a) Variance edge time slice at -1644 ms (b) Variance edge time slice at -3972

Rectilinear and sinusoidal. Conversely, the analysis of faults was done only in the inline seismic sections because it show a better and clearer footage of the fault geometries, dips and trends. A total of 15 faults were identify with none extending across the field. These fault are normal faults; listric, synthetic, antetic, horst, graben and collapse crest faults together with rollover anticlinal structure (Figures 7a, 6a, 6b, and 8). From the variance edge attribute maps (Figure 6a and 6b), most of the faults are soft link, attached sensing to each other but are not physically link (hard link) between their ends (relay wrap) thereby creating conduit for hydrocarbon migration. Some of these reservoir units have been displaced by faults with offset ranging between 2 ms and 100 ms (using conversion of 1 ms TWT = 1.12 m or 3.67 ft). Fault throws varies from 2.24 m (7.35 ft) to 112 m (167.45 ft) in the area, albeit fault offsets general decrease gradually to the younger sequences (reflectors at the top of the seismic section). Clinofolds are also present in the area and may form stratigraphic

traps (7b, 6a, and 6b). From variance attribute, channels and cutoff loops were identified, with channels levee characterized by high amplitude (indicates sand fill) and dipping in the NE-SW direction (Figures 7b and 6). The loop cutoffs (Figure 6a) shows the dynamic nature of the channels and indicates turbidity flow with high erosive energy. However, according Evans, (2003) low amplitude are correlated as shales or mudstone while high amplitudes indicate sand. Channel complexes are deep sea fan depositional features that may have been caused by turbidity current and are often related to floodplain fan and slope fan depositional facies environments. These channels are not horizontal because the time slice is not parallel to the channels but trail the dip of area.

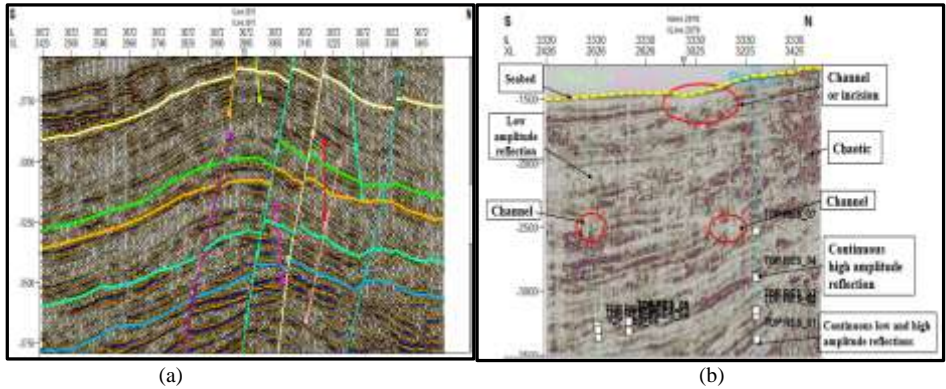


Figure 7: (a) Identification of Faults and Horizons (b) Seismic sequence and facies analysis

Qualitatively, the cause of change of amplitude versus offset was examined by tying reservoir tops, RES\_04 in Pira\_J-03 which is hydrocarbon bearing from well data to specific seismic reflectors on seismic data and comparing between near-angle stack and far-angle stack seismic (Figure 8a and 8b). From the observation, the variation of amplitude increased with distance (angle) at the reservoir tops showing the presence of hydrocarbon. And the section where no change in amplitude is observed indicates brine. This change in amplitude with offset due to fluid depicts class 3 AVO.

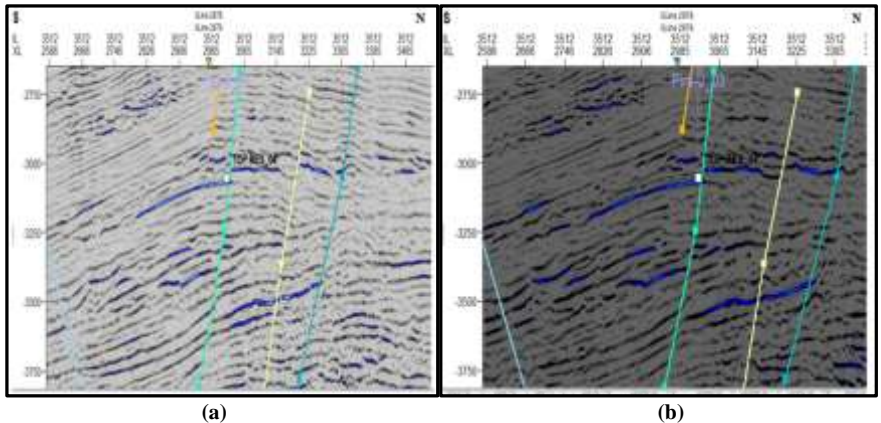


Figure 8 (a) Near-stack angle seismic section inline 3512 showing well and well top RES\_04 (b) Far-stack angle seismic section inline 3512 showing well top RES\_04

Out of the seven reservoir tops defined in well log analysis (Figure 3) only five reservoir tops (Figure 8a) were seismic stratigraphically correlated in both inclines and crosslines of the seismic section. Reservoir RES\_01, RES\_02, RES\_04, RES\_05 and RES\_07 tops time surface structural maps were produced to define the dips, trends and geometries of these reservoirs. The pastel pink color on the structural surface maps indicates structural low while the pastel red color indicates structural high. A second order polynomial function  $y = -276.279 + 1.63519 * x - 0.000360891 * x^2$  (Figure 9) was generated from the checkshot data to convert the

time structural maps into depth structural maps (Figures 10, 11, 12, 13, and 14). The position of structures, dips and trends on the depth surface structural maps were the same with the position in their time surface structural maps, thereby complementing the accuracy of the polynomial function.

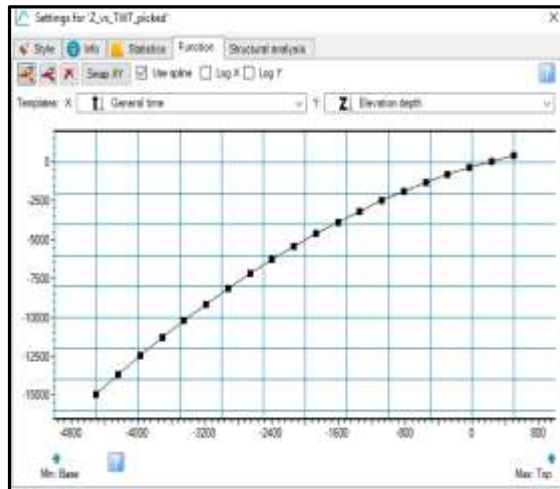


Figure 9: Polynomial function

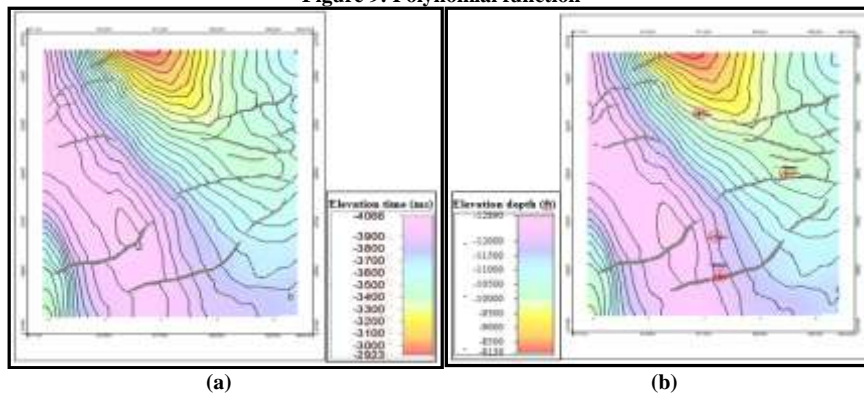


Figure 10: (a) RES\_01 Time structural surface map, (b) RES\_01 Depth structural surface map

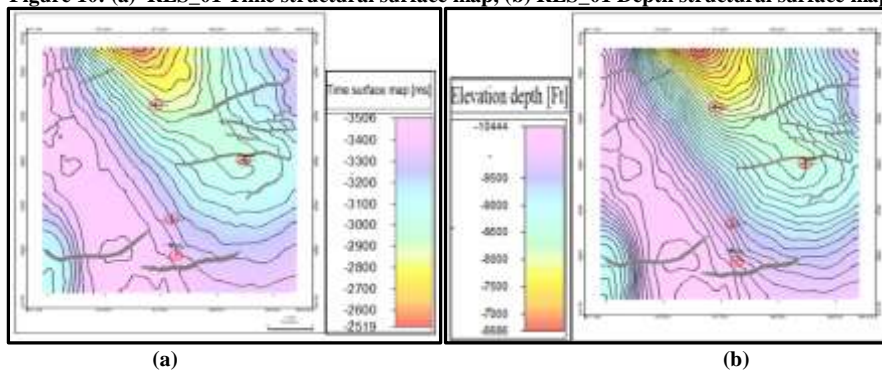


Figure 11: (a) RES\_02 Time structural surface map, (b) RES\_02 Depth structural surface map

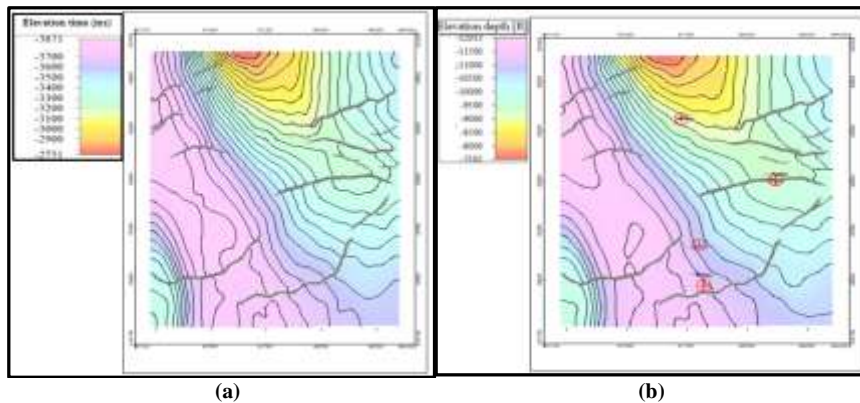


Figure 12: (a) RES\_04 Time structural surface map, (b) RES\_04 Depth structural surface map

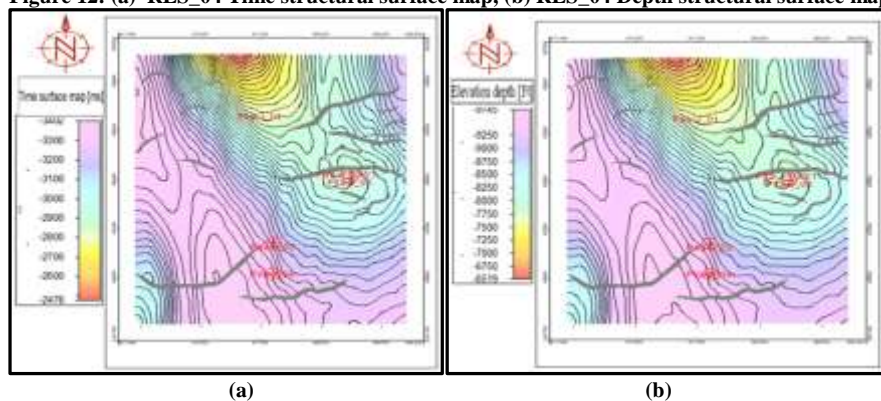


Figure 13: (a) RES\_05 Time structural surface map, (b) RES\_05 Depth structural surface map

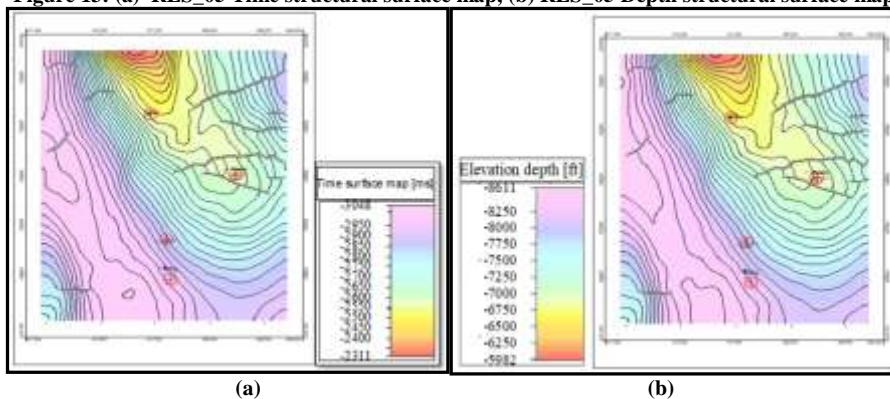


Figure 14: (a) RES\_07 Time structural surface map, (b) RES\_07 Depth structural surface map

#### Seismic attribute analysis

Seismic attributes, mathematically describes the characteristics or shape of a trace over a particular depth (time) window. RMS amplitudes and minimum amplitude attributes were extracted to relate the fluid and physical rock properties of the delineated reservoir intervals. This gave an idea of the type of fluid, lithogy, reservoir thickness, saturation and porosity. These attributes were extracted at two different angles and compared; near-angle stack RMS and minimum amplitudes and far-angle stack RMS and minimum attributes.

**Near-angle RMS and minimum amplitudes:** For near-angle stack amplitude, the attribute were generated from an angle of incident and reflection (where angle of incident equals angle of reflection) that is nearly zero

degree seismic (0 to 12 degree). This was used to define the lithology and fluid properties in the reservoir pore space. Near-angle stack RMS and minimum amplitude interval attribute map extractions were performed for each of the five reservoir intervals; RES\_01, RES\_02, RES\_04, RES\_05 and RES\_07 depicting channels (sand fairway) with clusters of bright amplitudes that are stratigraphically and structurally controlled. High RMS and low minimum amplitudes values relate to high porosity lithologies like sand and potentially, hydrocarbon zones. This means that these attributes are inversely proportional to one another.

**Far-angle RMS and minimum amplitudes:** Far-angle stack attribute for interval maps of RSM and minimum amplitude attributes were generated from 32 – 42 degree angle stack seismic. The results from the interval attributes for RES\_01, RES\_02, RES\_04, RES\_05 and RES\_07 are presented in figures 15, 16, 17, 18, and 19, where an increase in attribute intensity in the far-angle stack attributes were observed in all the five reservoir intervals.

Analyzing changes in amplitudes with offset (angles), the lithology and fluid effect at the reservoir can easily be spotted and scrutinize. This is because amplitude relates with fluid and physical properties of rock and is (reflection amplitude) also a function of offset and incidence angle. Examining both near and far-angle stack RMS and minimum amplitude respectively for each of reservoir intervals, whereby the attributes values increases with offset in RMS amplitudes and more negative in minimum amplitudes showed by the increase in color intensity in the reservoir fairways. These feature of amplitudes revealed in the reservoir intervals depict class 3 AVO (Amplitude Versus Offset) which occurs basically in tertiary sediments with high porosity values and sediments velocity greater than or equal to 5100 ft/sec which were all observed in this study.

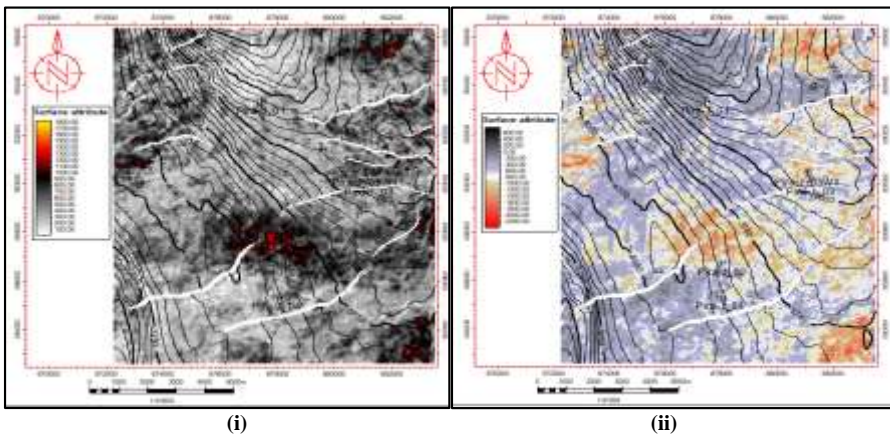


**Figure 15a: Near-angle stack (i) RMS amplitude and (ii) Minimum amplitude maps for RES\_01**

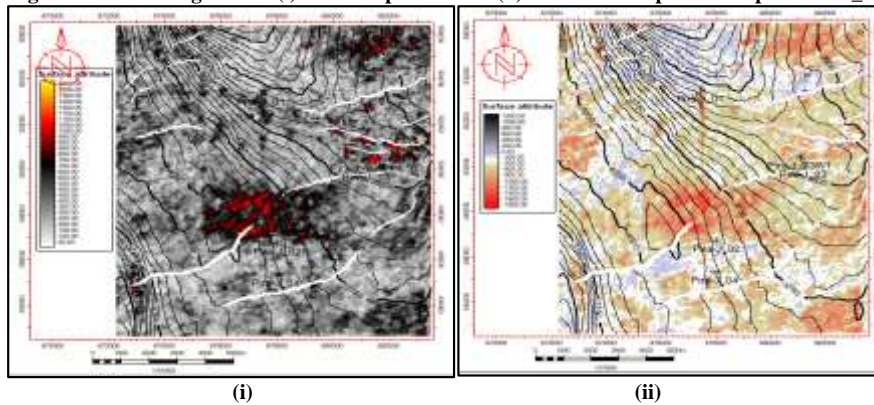


**Figure 15b: Far-angle stack (i) RMS amplitude and (ii) Minimum amplitude maps for RES\_01**

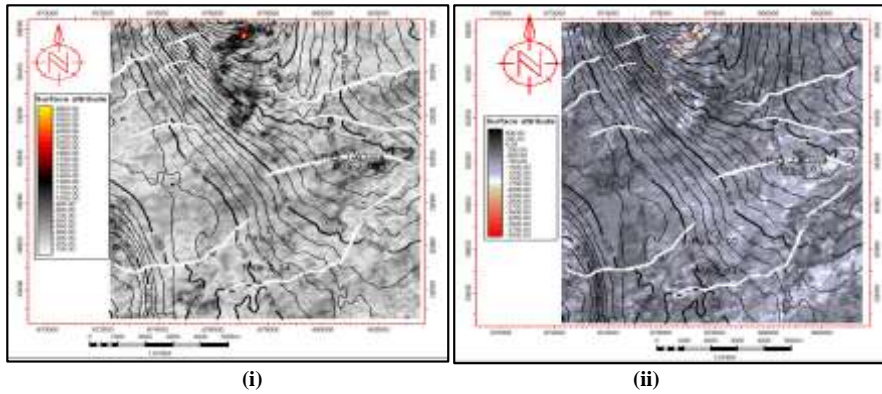


Figure 16a: Near-angle stack (i) RMS amplitude and (ii) Minimum amplitude maps for RES\_02

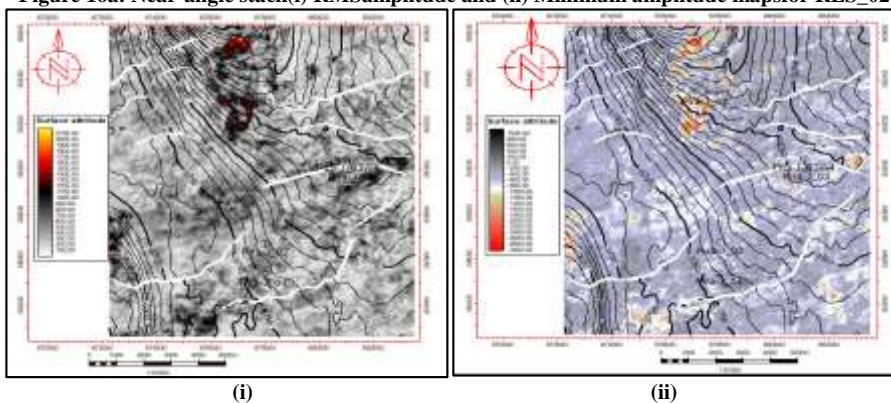


Figure 16b: Far-angle stack (i) RMS amplitude and (ii) Minimum amplitude maps for RES\_02

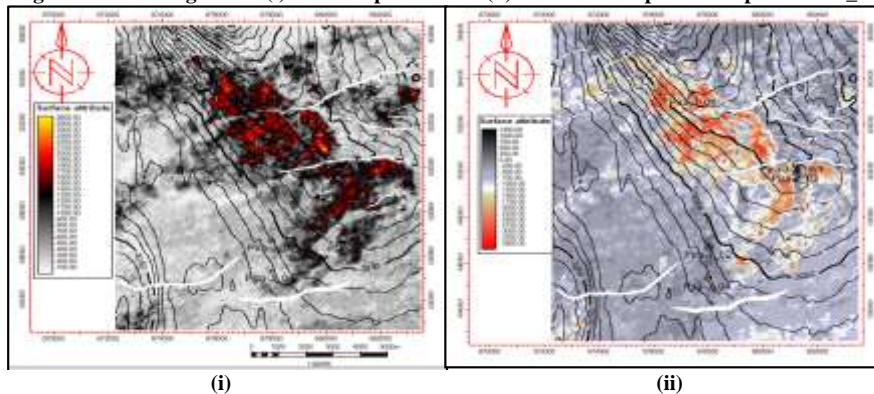


Figure 17a: Near-angle stack (i) RMS amplitude and (ii) Minimum amplitude maps for RES\_04

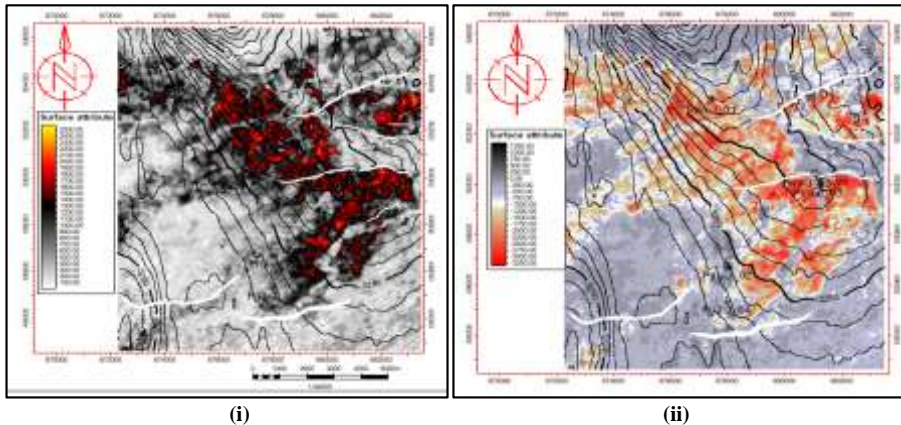
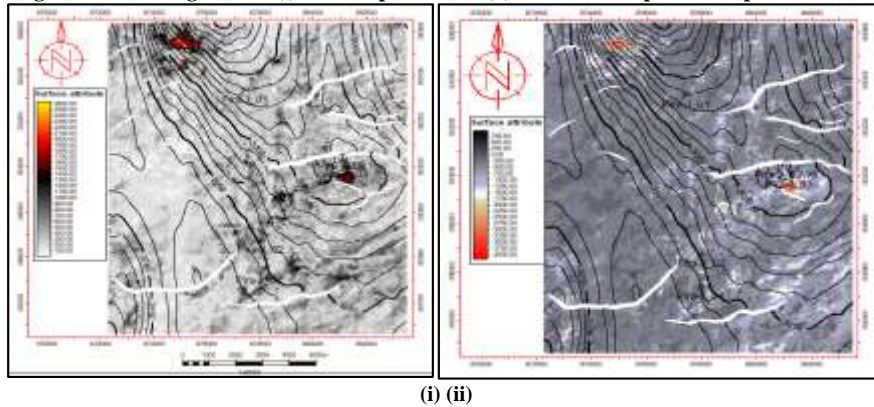


Figure 17b:Far-angle Stack (i)RMS amplitudeand (ii) Minimum amplitude maps for RES\_04



18a:Near-angle stack (i) RMS amplitude and (ii) Minimum amplitude maps for RES\_05

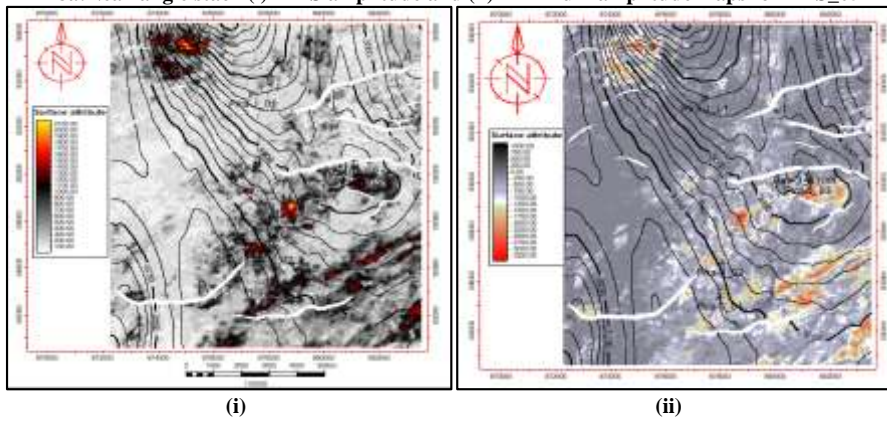


Figure 18b:Far-angle stack (i) RMS amplitude and (ii) Minimum amplitude maps for RES\_05

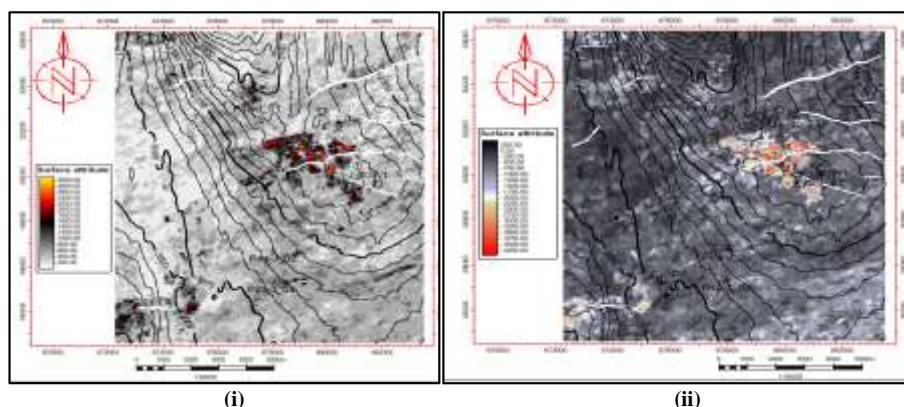


Figure 19a: Near-angle stack (i) RMS amplitude and (ii) Minimum amplitude maps RES\_07

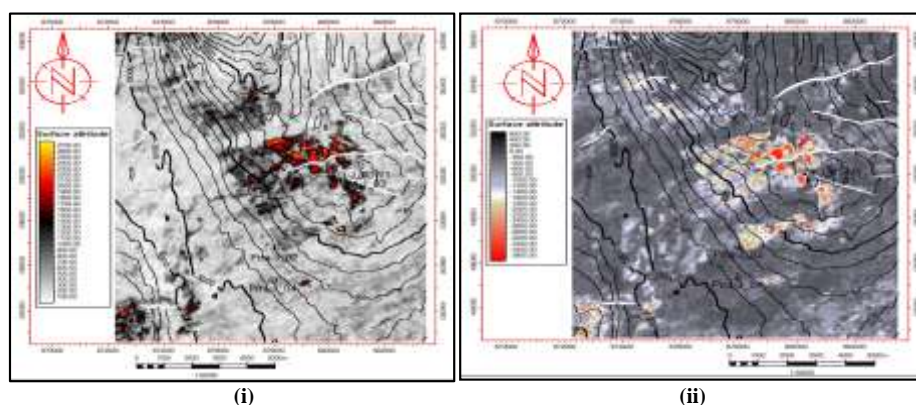


Figure 19: Far-angle stack (i) RMS amplitude and (ii) Minimum amplitude maps for RES\_07

#### IV. CONCLUSION AND RECOMMENDATIONS

The petrophysical analysis carried out in the 'Pira\_J' field deep water, offshore Niger Delta identified and defined seven reservoir units within a depth range of 6730.83 (22082.77 m) ft to 10445.1ft (34268.70 m). The reservoir units exhibited the following petrophysical properties ranges: average volume of shale: 0.10 to 0.44, average effective porosity: 0.14 to 0.34, average total porosity: 0.18 to 0.35, average hydrocarbon saturation: 0.5 to 0.9, average water saturation: 0.08 to 0.77, average net to gross ratio: 0.6 to 0.9, average permeability: 41.26 mD to 915.38 mD, average formation factor: 8.87 to 148.16 and average pore hydrocarbon volume: 0.12 to 0.85. Therefore, the field has quality reservoir properties. The results of this detailed definition of structural and stratigraphic pattern of the study area have shown that the deposited sediments were both structurally and stratigraphically controlled. This thus offers a better understanding of the trapping system, combination trap (stratigraphic and structural traps) of the field. Furthermore, seismic attributes show that the region contains significant accumulation of hydrocarbon depicted by the increase in RMS and decrease in minimum amplitudes intensity (brightness) from near-angle stack attributes to far-angle stack attributes. The petrophysical results were checked with seismic attributes and were seen to match with each other. Thus, integrating the petrophysical and attributes analysis displays that the 'Pira\_J' field hold significant volume of hydrocarbon, typically oil within the defined reservoir units with reservoir RES\_04 exhibiting the best reservoir qualities.

Therefore, it is suggested that fault seal analysis, seismic inversion and spectral analysis should be carried out in the study area. This will depict a better understanding of the sealing potential of the traps, image the rock elastic and physical properties (porosity, fluid content and lithology), boundaries of the channels axes, splays and margins.

### References

- [1]. Archie, G. E. (1942). The electrical reservoir log as an aid in determining some reservoir characteristics. *Trans AME*, 146(19), 54-64.
- [2]. Avbovo, A. (1978). Tertiary lithostratigraphy of the Niger Delta. *AAPG Bulletin*, 62, 295-300.
- [3]. Bell, J. M., Chin, Y. D., & Hanrahan, S. (2005). State-of-the-art of ultra deepwater production technologies. In: *Offshore technology conference*. doi:3. Bell JM, Chin YD, Hanrahan S (2005). State-of-the-art of ultra dorg/10.4043/17615 -MS
- [4]. Bodine, J. H. (1984). Waveform analysis with seismic attributes. *SEG 54th Annual International Meeting*, Atlanta.
- [5]. Bodine, J. H. (1986). Waveform analysis with seismic attributes. *Oil Gas Journal*, 84(24), 59-63.
- [6]. Burke, K. (1972). Longshore drift, submarine canyons, and submarine fans in development of Niger Delta: . *AAPG Bulletin* , 56, 1975- 1983.
- [7]. Chopra S, M. K. (2005). Attribute review paper. 75th Ann of SEG: Draft 3., 51.
- [8]. Doust, H., & Omatsola, E. (1990.). Niger Delta in divergent/passive margin basins, in J. D. Edwards and P. A. Santogrossi, eds. *AAPG Memoir*, 48, 201-238.
- [9]. Dresser, A. (1979). *Log interpretation Charts*. Inc. 1-10. Houston Dresser Industries, 1-10.
- [10]. EIA. (2018). 'International energy outlook 2018'. Retrieved February 23, 2023, from [https:// www.eia.gov/ outlooks/ ieo/](https://www.eia.gov/outlooks/ieo/)
- [11]. Evamy, B. O., Herembourne, J., Kameline, P., Knap, W. A., Molloy, F. A., & Rowlan. (1978). Hydrocarbon habitat of Tertiary Niger Delta. *American Association of Petroleum Geologists Bulletin*, 62, 1-39.
- [12]. Evans, D. (2003). *Shallow Clues for Deep Exploration* . *Oilfield Review*, Winter, 2-3.
- [13]. ExxonMobil. (2018). '2018 outlook for energy: A view to 2040'. Retrieved January 15, 2023, from [http:// cdn.exxonmobil.com/ ~/ media/ global/ files/ outlook-for-energy/ 2018/ 2018- outlook-for-energy.pdf](http://cdn.exxonmobil.com/~media/global/files/outlook-for-energy/2018/2018-outlook-for-energy.pdf)
- [14]. ExxonMobil. (2022). '2022 outlook for energy executive summary. Retrieved January 20, 2023
- [15]. Joye, S. B. (2015). Deepwater Horizon, 5 years on. *Science*, 349(6248), 592-593.
- [16]. Kulke, H. (1995). Nigeria, in H. Kulke, ed., *Regional petroleum geology of the world: Part II. Africa, America, Australia and Antarctica*: Berlin, Gebru' der Borntraeger. 143- 172.
- [17]. Lawrence, S. R., Monday, S., & Bray.R. (2002). Regional geology and geophysics of the eastern Gulf of Guinea (Niger Delta to Rio Muni). *The Leading Edge*, 21(11), 1112-1117.
- [18]. Lehner, P., & De Ruiter, P. A. C. (1977). Structural history of Atlantic margin of Africa. *AAPG Bulletin*, 61, 961- 981.
- [19]. Nations, U. (2017, January 20). 'World population prospects: The 2017 revision'.
- [20]. Onuoha, K. M. (1999). Structural features of Nigeria's coastal margin: An assessment base of age data from wells . *Journal of African Earth Sciences*, 29, 485-499.
- [21]. Petroleum, B. (2018). *Bp energy outlook: 2018 edition*.
- [22]. Reader, T. W., & O'Connor, P. . (2014). The Deepwater Horizon explosion: non-technical skills, safety culture, and system complexity. *J Risk Res*, 17(3), 405-424.
- [23]. Short K, & Stauble, A . (1967). Outline of geology of Niger delta. *Am Assoc Pet Geol Bull*, 51, 761-779.
- [24]. Skogdalen, J. E., & Vinnem, J. E. . (2012). Quantitative risk analysis of oil and gas drilling, using Deepwater Horizon as case study. *Reliab Eng Syst Saf*, 100, 58-66.
- [25]. Stacher, P. (1995). Present understanding of the Niger Delta hydrocarbon habitat, in, Oti, M.N., and Postma, G., eds., *Geology of Deltas*. Rotterdam, A.A. Balkema, , 257-267.
- [26]. Taner, M. T. (2001). Seismic attributes. *CSEG Recorder*(September Issue), 48-56.
- [27]. Taner, M. T., Schuelke, J. S., O'Doherty, R. , & Baysal, E. (1994). Seismic attributes revisited. 64th Annual International Meeting, SEG, Expanded Abstracts. 1104 - 1106.
- [28]. Wu, S., & Bally, A. W. (2000). Slope tectonics— Comparisons and contrasts of structural styles of salt and shale tectonics of the northern Gulf of Mexico with shale tectonics of offshore Nigeria in Gulf of Guinea, in W. Mohriak and M. Talwani, eds., *Atlantic rifts and continental margi*. *American Geophysical Union*, 151- 172.